[redacted]

Copy 212
RM L55F09

NACA RM L55F09

USAF TECHNICAL LIBRARY
HOLLOMAN AIR FORCE BASE
ALAMOGORDO, NEW MEXICO

NACA
RM
L55F09
c.212

LOAN COPY. RETURN TO
TECHNICAL LIBRARY
AIR FORCE WEAPONS LAB.

TECH LIBRARY KAFB, NM
0144110

NACA

RESEARCH MEMORANDUM

THEORETICAL INVESTIGATION OF LAMINAR HEAT TRANSFER ON YAWED INFINITE CYLINDERS IN SUPERSONIC FLOW AND A COMPARISON WITH EXPERIMENTAL DATA

By Ivan E. Beckwith

Langley Aeronautical Laboratory
Langley Field, Va.

CLASSIFIED DOCUMENT

This material contains information affecting the National Defense of the United States within the meaning of the espionage laws, Title 18, U.S.C., Secs. 793 and 794, the transmission or revelation of which in any manner to an unauthorized person is prohibited by law.

NATIONAL ADVISORY COMMITTEE
FOR AERONAUTICS

WASHINGTON

August 9, 1955

[redacted]

1Z

 [redacted]

TECH LIBRARY KAFB, NM
0144110

NATIONAL ADVISORY COMMITTEE FOR AERONAUTICS

RESEARCH MEMORANDUM

THEORETICAL INVESTIGATION OF LAMINAR HEAT TRANSFER ON YAWED INFINITE CYLINDERS IN SUPERSONIC FLOW AND A COMPARISON WITH EXPERIMENTAL DATA

By Ivan E. Beckwith

SUMMARY

A theoretical method is presented for the calculation of heat transfer in the laminar boundary layer on yawed infinite cylinders in compressible flow with a Prandtl number near unity. The method may be applied to a cylinder of arbitrary cross section and arbitrary chordwise wall-temperature distribution. General expressions are derived for the heat transfer and recovery factor in the vicinity of the stagnation line. The expression for the recovery factor and the chordwise velocity profile at the stagnation line for zero heat transfer are in good agreement with the results of other theoretical analyses.

The method is appl[redacted] the calculation of local heat-transfer rates on a yawed circular cylinder at a stream Mach number of 6.9. Comparison of the results of this calculation with some experimental data indicates good agreement for small yaw angles but at the larger yaw angles of 60° or more the theoretically predicted heat transfer is about 40 percent less than the measured values.

INTRODUCTION

As flight speeds are increased, the problem of aerodynamic heating becomes more acute and requires that every possible means be investigated for alleviating the heat transfer at critical locations on missile or aircraft configurations. One such critical location is a sharp leading edge or nose where the local heat transfer becomes very large because of the thin boundary layer which has just begun to form. Appreciable reductions in heat transfer to the forward regions of wings and bodies may therefore be obtained by rounding or blunting the leading edge or nose. (Another advantage of a blunt entry section over a sharp section is that heat may be removed more effectively from the blunt section by heat conduction or internal cooling). Recent theoretical and experimental

[redacted]

[redacted]

investigations (refs. 1 to 4) as well as early experimental results (ref. 5) have indicated that further reductions in heat transfer to blunt leading edges can be obtained by yawing or sweeping the wing.

Inspection of the laminar boundary-layer equations for a yawed infinite cylinder in an incompressible flow with a Prandtl number of unity and negligible viscous heating shows that both the chordwise flow and the temperature distribution are not affected by yawing the cylinder (ref. 1), that is, the temperature and chordwise velocity distributions are independent of the spanwise flow component. The solution for this case (ref. 2) then shows that the heat transfer decreases as the square root of the cosine of the yaw angle. This decrease in heat transfer is due to the increase in boundary-layer thickness which occurs at a given point on the cylinder as the yaw angle is increased.

In a compressible flow the independence principle for the yawed, infinite cylinder no longer applies since shear stresses associated with the spanwise flow will affect the temperature distribution directly, as well as affecting the chordwise velocity profiles through the resulting density changes, (refs. 6 to 8). An analytic solution of the general problem of heat transfer to yawed infinite cylinders in compressible flow is at present virtually impossible so that recourse must be had to an approximate solution such as can be obtained from a suitable extension of the integral methods (refs. 9 to 12). The range of validity and accuracy of a solution of this type cannot be determined without comparison with mathematically exact solutions or experimental data. As far as is known, the only exact solution available for the compressible flow problem is Crabtree's (ref. 8) in which the differential equations for Prandtl number unity and zero heat transfer are solved in a linearized form.

The purpose of the present paper is to present a theoretical investigation of the compressible laminar boundary layer on yawed infinite cylinders and to compare the results with some experimental data showing the effect of yaw on the heat transfer to a simulated leading edge (ref. 3). The theoretical analysis is based on an integral method wherein a linear viscosity temperature relation is used and the boundary layer is assumed to have one thickness. The latter assumption simplifies the calculations considerably since the simultaneous solution of only two differential equations is required to obtain the local heat-transfer rates. A more general method would involve the simultaneous solution of three differential equations; one for the thermal boundary-layer thickness, and two more for the boundary-layer thicknesses corresponding to the chordwise and spanwise components of the velocity boundary layer.

SYMBOLS

x	boundary-layer coordinate parallel to surface, normal to cylinder axis
y	boundary-layer coordinate parallel to surface and cylinder axis
z	boundary-layer coordinate normal to cylinder surface
t	time
ρ	mass density
u	velocity in x-direction
v	velocity in y-direction
w	velocity in z-direction
p	pressure
μ	dynamic viscosity
ν	kinematic viscosity
h	static enthalpy, c_pT
k	thermal conductivity
T	static temperature, $^{\circ}R$
T^*	stagnation temperature, $^{\circ}R$
T_e	recovery temperature for local $q_w = 0$
H	stagnation enthalpy (eq. 6)
σ	Prandtl number, $\frac{c_p\mu}{k}$
c_p	specific heat at constant pressure
R	constant in equation of state for gases
η	Dorodnitzyn variable (eq. 10)

ρ^* local stagnation density

Δ boundary-layer thickness in η coordinate system

$\eta^* = \frac{\eta}{\Delta}$

$t^* = H - H_w = H - c_p T_w$

$\bar{t} = \frac{t^*}{t_1^*} = \frac{H - c_p T_w}{H_1 - c_p T_w}$, thermal-profile parameter

S Sutherland constant

λ chordwise velocity-profile parameter (eq. (15))

$B_1, B_2, B_3 \ldots$ coefficients in thermal profile (eq. (18))

θ momentum thickness in η coordinate system (eq. (22))

δ^* displacement thickness in η coordinate system (eq. (23))

Δ^* thermal-profile parameter (eq. (26))

φ energy-loss-profile parameter (eq. (27))

$\alpha_0, \alpha_1, \alpha_2 \ldots$ constants in expression for φ (eq. (28))

M_1 local chordwise Mach number external to boundary layer

q_w local heat-transfer rate at wall (negative for heat transfer to wall)

L characteristic dimension of body

U_N velocity component normal to cylinder axis on stagnation streamline ahead of cylinder

U_∞ resultant velocity ahead of bow shock (flight velocity of cylinder)

M_∞ resultant Mach number ahead of bow shock

$\bar{x} = x/L$

β yaw angle of cylinder (measured from a line normal to resultant stream direction)

F function of λ and $\frac{T_w}{T_{l_0}}$ (eq. (43))

M_N chordwise component of Mach number on stagnation streamline ahead of cylinder

C_p pressure coefficient

D diameter of circular cylinder

γ ratio of specific heats, 1.400 used throughout

h_c local heat-transfer coefficient

$\bar{h}_c$ average heat-transfer coefficient

R_{S_L} reference Reynolds number, $\frac{\rho_s U_{N_s} L}{\mu_s}$

Z, ϕ computing parameters (eqs. (A3) and (A4))

Subscripts:

l local conditions external to boundary layer unless otherwise noted

w conditions at wall

∞ conditions ahead of bow shock

s conditions just behind normal bow shock

l_0 conditions external to boundary layer at stagnation line

THEORY

Derivation of the Integral Equations

The boundary-layer equations for a three-dimensional flow are obtained by application of the conventional boundary-layer assumptions to the general equations governing the motion of a compressible, viscous, heat-conducting gas (refs. 7 and 13). Two of these assumptions which may be emphasized for the present application are (1) the boundary-layer thickness is small compared with some characteristic dimension of the body, and (2) the pressure gradient normal to the surface may be neglected provided that the boundary-layer thickness is small compared with the local radius of curvature of the surface. Thus, for example, the boundary-layer equations are expected to be valid everywhere on a circular cylinder except in a separated region provided that the stream Reynolds number based on diameter (or radius of curvature of the leading edge) is large.

The boundary-layer equations for steady flow on an infinite yawed cylinder are obtained from the three-dimensional equations with $\frac{\partial}{\partial t} = 0$ and $\frac{\partial}{\partial y} = 0$. The boundary-layer coordinate system used is defined by the following sketch:

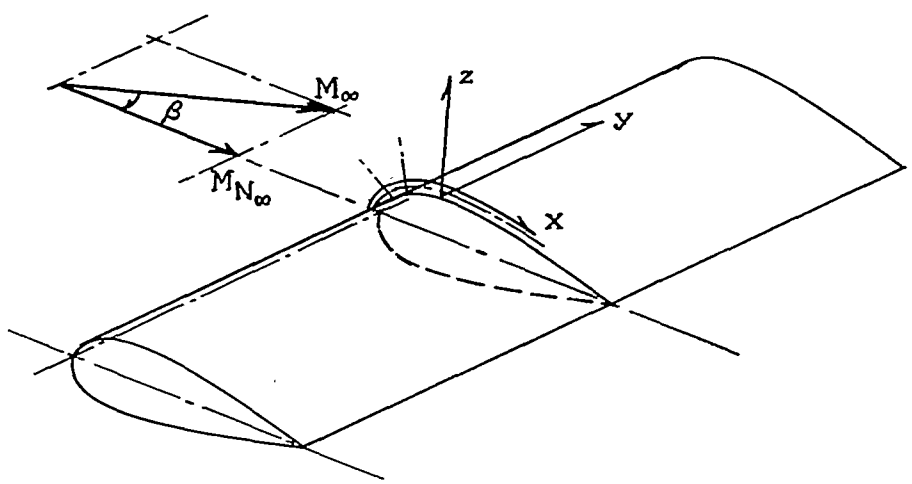

The equation of continuity is then

$$\frac{\partial}{\partial x}(\rho u) + \frac{\partial}{\partial z}(\rho w) = 0. \tag{1}$$

and the equations of motion in the x-, y-, and z-directions are written as

$$\rho u\frac{\partial u}{\partial x} + \rho w\frac{\partial u}{\partial z} = -\frac{\partial p}{\partial x} + \frac{\partial}{\partial z}\left(\mu\frac{\partial u}{\partial z}\right) \tag{2}$$

$$\rho u\frac{\partial v}{\partial x} + \rho w\frac{\partial v}{\partial z} = \frac{\partial}{\partial z}\left(\mu\frac{\partial v}{\partial z}\right) \tag{3}$$

$$0 = \frac{\partial p}{\partial z} \tag{4}$$

where z is normal to the surface. The energy equation is written as

$$\rho u\frac{\partial h}{\partial x} + \rho w\frac{\partial h}{\partial z} = u\frac{\partial p}{\partial x} + \frac{\partial}{\partial z}\left(k\frac{\partial T}{\partial z}\right) + \mu\left[\left(\frac{\partial u}{\partial z}\right)^2 + \left(\frac{\partial v}{\partial z}\right)^2\right] \tag{5}$$

Then, for convenience, a stagnation enthalpy is defined as

$$H = h + \frac{u^2}{2} + \frac{v^2}{2} \tag{6}$$

whereupon equations (2), (3), and (5) may be combined to yield

$$\rho u\frac{\partial H}{\partial x} + \rho w\frac{\partial H}{\partial z} = \frac{\partial}{\partial z}\left(\mu\frac{\partial H}{\partial z}\right) + \left(\frac{1}{\sigma} - 1\right)\frac{\partial}{\partial z}\left(\mu\frac{\partial h}{\partial z}\right) \tag{7}$$

for constant c_p and σ. The chordwise pressure gradient impressed on the boundary layer is obtained from equation (2) evaluated outside the boundary layer, that is, outside the region where viscous effects are important, as

$$\rho_1 u_1 \frac{du_1}{dx} = -\frac{dp}{dx} \tag{8}$$

which is Bernoulli's equation. The equation of state for a perfect gas

$$p = \rho RT \tag{9}$$

is used throughout.

Equations (2) and (7) are integrated across the boundary layer (as in ref. 11) and by using equations (1), (4), (8), and (9), together with the Dorodnitzyn variable

$$\eta = \int_0^z \frac{\rho}{\rho_1^*} dz \tag{10}$$

the results may be expressed as

$$\frac{d}{dx}\left[\Delta \int_0^1 \left(\frac{u}{u_1} - \frac{u^2}{u_1^2}\right) d\eta^*\right] + \left[2\Delta \int_0^1 \left(\frac{u}{u_1} - \frac{u^2}{u_1^2}\right) d\eta^* + \Delta \int_0^1 \left(\frac{\rho_1}{\rho} - \frac{u}{u_1}\right) d\eta^*\right] \frac{1}{u_1} \frac{du_1}{dx} = \frac{\mu_w \rho_w}{u_1 \rho_1^{*2} \Delta} \left(\frac{\partial}{\partial \eta^*} \frac{u}{u_1}\right)_w \tag{11}$$

and

$$\frac{d}{dx}\left[\Delta \int_0^1 \frac{u}{u_1}(1 - \bar{t}) d\eta^*\right] + \left(\frac{1}{u_1} \frac{du_1}{dx} - \frac{c_p}{t_1^*} \frac{dT_w}{dx}\right) \Delta \int_0^1 \frac{u}{u_1}(1 - \bar{t}) d\eta^* = \frac{\mu_w \rho_w}{\sigma \rho_1^{*2} u_1 \Delta} \left(\frac{\partial \bar{t}}{\partial \eta^*}\right)_w \tag{12}$$

for the boundary conditions at $\eta^* = 0$ of $u = 0$, $v = 0$, $w = 0$, and $\bar{t} = 0$ and at $\eta^* = 1$, $u = u_1$, $v = v_1$, $\bar{t} = 1$, and $\frac{\partial}{\partial \eta^*} = 0$ where Δ is a universal boundary-layer thickness. Note that these equations are of exactly the same form as the corresponding equations of reference 11 for two-dimensional flow. The spanwise component of the flow, however, is involved directly in the density-ratio integral of equation (11) and in the stagnation enthalpy integrals of equation (12) as will be shown later.

Velocity and Enthalpy Profiles

An approximate solution to equations (11) and (12) becomes possible after specifying the velocity and enthalpy profiles. The chordwise velocity profile will be described by the conventional fourth-degree polynomial in $\eta^* = \frac{\eta}{\Delta}$. A fourth-degree polynomial is then used for the spanwise velocity profile in order to satisfy the requirement that both profiles must be of the same shape in the limiting case of a yawed flat plate. The stagnation enthalpy profile will be expressed as a fifth-degree polynomial which has resulted in acceptable engineering accuracy for the heat transfer to an unyawed cylinder when $T_w < T_e$ (ref. 11). The coefficients of all profiles are determined from specified conditions at the edge of the boundary layer ($\eta = \Delta$) and at the wall ($\eta = 0$) so that the original equations of motion (eqs. (1) to (7)), after being transformed to the new variable η, are satisfied when evaluated at the wall.

The profile coefficients can be simplified if a viscosity-temperature relation of the form

$$\mu = \frac{\mu_w}{T_w} T \tag{13}$$

is assumed where the quantity $\frac{\mu_w}{T_w}$ is a function only of x with μ_w determined from the given values of T_w by any acceptable method such as Sutherland's viscosity-temperature equation. In the following derivation, equation (13) is actually used in the vicinity of the wall only, and, as will be seen, the final results in the form of a heat-transfer coefficient, for example, are automatically expressed in terms of μ_w and k_w where k_w may also be evaluated from T_w according to the best available information. In the practical application of these results or for the purpose

of comparison with experimental data, however, it is usually desirable to use a reference viscosity and conductivity such as μ_∞ and k_∞. Consequently, the problem arises as to the proper evaluation of the ratios μ_w/μ_∞ or k_w/k_∞. According to the above considerations, and since μ_∞ and k_∞ never enter the basic derivation, the viscosity ratio should be obtained from the Sutherland equation which would be written as

$$\frac{\mu_w}{\mu_\infty} = \left(\frac{T_w}{T_\infty}\right)^{3/2}\frac{T_\infty + S}{T_w + S}$$

The conductivity ratio should also be determined from equally accurate information.

The chordwise velocity profile may now be written as (ref. 11)

$$\frac{u}{u_1} = \frac{12 + \lambda}{6}\eta^* - \frac{\lambda}{2}(\eta^*)^2 + \frac{3\lambda - 12}{6}(\eta^*)^3 + \frac{6 - \lambda}{6}(\eta^*)^4 \tag{14}$$

which satisfies the conditions at $\eta^* = 1$ that

$$\frac{u}{u_1} = 1$$

$$\frac{\partial}{\partial\eta^*}\left(\frac{u}{u_1}\right) = 0$$

$$\frac{\partial^2}{\partial\eta^{*2}}\left(\frac{u}{u_1}\right) = 0$$

The relation for λ is obtained from equation (2) (transformed to η and evaluated at $\eta = 0$) as

$$\lambda = \frac{\rho_1}{\mu_w}\left(\frac{\rho_1^*}{\rho_w}\right)^2 \frac{du_1}{dx} \Delta^2 \tag{15}$$

after also using equations (4), (8), (9), and (13).

Application of the same procedure to equation (3) shows that, at $\eta = 0$,

$$\frac{\partial^2}{\partial \eta^{*2}}\left(\frac{v}{v_1}\right) = 0 \tag{16}$$

Hence, the required spanwise profile can be written as

$$\frac{v}{v_1} = 2\left(\eta^*\right) - 2\left(\eta^*\right)^3 + \left(\eta^*\right)^4 \tag{17}$$

which at $\eta^* = 1$ gives

$$\left(\frac{v}{v_1}\right) = 1$$

$$\frac{\partial}{\partial \eta^*}\left(\frac{v}{v_1}\right) = 0$$

$$\frac{\partial^2}{\partial \eta^{*2}}\left(\frac{v}{v_1}\right) = 0$$

Comparison of equation (17) with equation (14) shows that, for a flat plate ($\lambda = 0$), the two profiles become identical as would be expected.

The stagnation enthalpy profile is written as

$$\frac{t^*}{t_1^*} = \bar{t} = B_1\eta^* + B_2\left(\eta^*\right)^2 + B_3\left(\eta^*\right)^3 + B_4\left(\eta^*\right)^4 + B_5\left(\eta^*\right)^5 \tag{18}$$

where the boundary conditions at $\eta^* = 1$ are taken as

$$\bar{t} = 1$$

$$\frac{\partial\bar{t}}{\partial\eta^*} = 0$$

with the result that

$$\left.\begin{aligned} B_4 &= 5 - 4B_1 - 3B_2 - 2B_3 \\ B_5 &= -4 + 3B_1 + 2B_2 + B_3 \end{aligned}\right\} \tag{19}$$

The coefficient B_2 is derived from equation (7) which is transformed to the x, η coordinates and evaluated at the wall ($u = 0$, $w = 0$). The result can be expressed as

$$B_2 \equiv \frac{1}{2}\left(\frac{\partial^2\bar{t}}{\partial\eta^{*2}}\right)_{\eta=0} = \frac{1 - \sigma}{2t_1^*}\left[\left(\frac{12 + \lambda}{6}\right)^2 u_1^2 + 4v_1^2\right] \tag{20}$$

after using equations (4), (9), and (13) and the definitions of H and $\bar{t}$. The first derivatives of the velocity profiles are obtained from equations (14) and (17).

The third thermal profile coefficient B_3 is derived from the first derivative with respect to η of equation (7) (expressed in the x, η coordinate system) evaluated at the wall. In order to obtain the final expression for B_3, as given below, note that $\left(\frac{\partial w}{\partial \eta}\right)_{\eta=0} = 0$ and $\left(\frac{\partial \eta}{\partial x}\right)_{\eta=0} = 0$ from equations (1) and (10), respectively. Also equations (15) and (20) have been used to supply expressions for Δ^2 and the quantity $\left[\left(\frac{\partial u}{\partial \eta}\right)^2 + \left(\frac{\partial v}{\partial \eta}\right)^2\right]_{\eta=0}$. The result may be written as

$$B_3 \equiv \frac{1}{6}\left(\frac{\partial^3 t}{\partial \eta^{*3}}\right)_{\eta=0} = \frac{u_1}{t_1^*}\,\frac{12\lambda + \lambda^2}{36}\left[\sigma c_p \frac{T_1}{T_w}\,\frac{\frac{dT_w}{dx}}{\frac{du_1}{dx}} - 3(1 - \sigma)u_1\right] \tag{21}$$

where derivatives of the velocity profiles from equations (14) and (17) have been used where necessary. The coefficient B_1 in equation (18) will be determined from the solution of the integral equations.

Expression of Profile Integrals in Terms of λ and B_1

The various profile integrals in equations (11) and (12) can now be evaluated in terms of λ and B_1 which are the two basic parameters to be determined from the simultaneous solution of these two equations.

Thus, from equation (14) and the definition of a momentum thickness in the η coordinate system, there is obtained

$$\frac{\theta}{\Delta} = \int_0^1 \left(\frac{u}{u_1} - \frac{u^2}{u_1^2}\right) d\eta^* = \frac{1}{315}\left(37 - \frac{\lambda}{3} - \frac{5\lambda^2}{144}\right) \tag{22}$$

Similarly, a displacement thickness in the x, η plane (analogous to the displacement thickness in incompressible flow) is expressed as

$$\frac{\delta^*}{\Delta} = \int_0^1 \left(1 - \frac{u}{u_1}\right) d\eta^* = \frac{36 - \lambda}{120} \tag{23}$$

Then from the definition of H and $\bar{t}$ and the relation $\frac{\rho_1}{\rho} = \frac{T}{T_1}$, the density integral may be expressed as

$$\int_0^1 \left(\frac{\rho_1}{\rho} - \frac{u}{u_1}\right) d\eta^* = \frac{T_1^*}{T_1}\left(\frac{T_w}{T_1^*} - 1\right)\frac{\Delta^*}{\Delta} + \frac{u_1^2}{2c_pT_1}\frac{\theta}{\Delta} +$$

$$\left(1 + \frac{u_1^2}{2c_pT_1}\right)\frac{\delta^*}{\Delta} + \frac{v_1^2}{2c_pT_1}\int_0^1 \left(1 - \frac{v^2}{v_1^2}\right) d\eta^* \tag{24}$$

by means of equations (22) and (23). The last integral on the right in equation (24) becomes by virtue of equation (17)

$$\int_0^1 \left(1 - \frac{v^2}{v_1^2}\right) d\eta^* = \frac{263}{630} \tag{25}$$

The integral expression $\frac{\Delta^*}{\Delta}$ in equation (24) is evaluated from equations (18) and (19) as

$$\frac{\Delta^*}{\Delta} = \int_0^1 (1 - \bar{t}) d\eta^* = \frac{2}{3} - \frac{1}{5}B_1 - \frac{1}{15}B_2 - \frac{1}{60}B_3 \tag{26}$$

where equations (20) and (21) are used to express B_2 and B_3 as functions of λ. The integral term in equation (12) is evaluated in the same way and yields

$$\frac{\varphi}{\Delta} = \int_0^1 \frac{u}{u_1}(1 - \bar{t})d\eta^* = \alpha_0 + \frac{\lambda}{6}\alpha_4 + \left(\alpha_1 + \frac{\lambda}{6}\alpha_5\right)B_1 +$$

$$\left(\alpha_2 + \frac{\lambda}{6}\alpha_6\right)B_2 + \left(\alpha_3 + \frac{\lambda}{6}\alpha_7\right)B_3 \tag{27}$$

The values of the α's depend only on the type of thermal profile used and are listed below for the fifth-degree profile used here.

$$\left.\begin{aligned} \alpha_0 &= 0.38175 & \alpha_4 &= 0.04484 \\ \alpha_1 &= -0.14603 & \alpha_5 &= -0.01230 \\ \alpha_2 &= -0.05317 & \alpha_6 &= -0.00357 \\ \alpha_3 &= -0.01389 & \alpha_7 &= -0.00079 \end{aligned}\right\} \tag{28}$$

Equations (11) and (12) may now be written in a more convenient form by introducing equations (22), (23), (24), (25), (26), and (27); thus,

$$\frac{d\theta}{dx} + \frac{\theta}{u_1}\frac{du_1}{dx}\left[2 + \frac{\gamma - 1}{2}M_1^2 + \left(1 + \frac{\gamma - 1}{2}M_1^2\right)\frac{\delta^*}{\theta} + \right.$$

$$\left.\frac{T_1^*}{T_1}\left(\frac{T_w}{T_1^*} - 1\right)\frac{\Delta^*}{\theta} + \frac{263}{630}\frac{\Delta}{\theta}\frac{v_1^2}{2c_pT_1}\right] = \frac{\mu_w\rho_w}{u_1(\rho_1^*)^2\Delta}\frac{12 + \lambda}{6} \tag{29}$$

and

$$\frac{d\varphi}{dx} + \left(\frac{1}{u_1}\frac{du_1}{dx} - \frac{c_p}{t_1^*}\frac{dT_w}{dx}\right)\varphi = \frac{\mu_w\rho_w}{\sigma(\rho_1^*)^2u_1\Delta}B_1 \tag{30}$$

where

$$M_1 = \frac{u_1}{\sqrt{\gamma R T_1}}$$

The external spanwise velocity v_1 may be expressed as a function of temperature and the local chordwise Mach number M_1 as

$$\frac{v_1^2}{2c_p T_1} = \frac{T_1^*}{T_1} - \left(1 + \frac{\gamma - 1}{2} M_1^2\right) \tag{31}$$

In principle, equations (29) and (30) can now be solved for λ and B_1 by a suitable numerical procedure for any given distribution of u_1 and T_w. Before the computation can be started, however, the initial values and first derivatives at $x = 0$ of λ and B_1 must be known. (See appendix.)

General Expression for the Local Heat Transfer

The local convective heat-transfer rate is defined as

$$q_w = -k_w \left(\frac{\partial T}{\partial z}\right)_w$$

Introducing the transformation to η^* and using equations (15) and (18) and the definition of t^* result in

$$q_w = -k_w \left(T_1^* - T_w\right) \left(\frac{du_1}{dx} \frac{\rho_1}{\mu_w}\right)^{1/2} \frac{B_1}{\sqrt{\lambda}} \tag{32}$$

A heat-transfer parameter which depends only on the yaw angle for given stream conditions and wall temperature is then obtained from equation (32) as

$$\frac{q_w L}{k_w\left(T_w - T_1^*\right)\sqrt{\frac{\rho_s U_{N_s} L}{\mu_w \cos\beta}}} = \left[\cos\beta\left(\frac{d}{d\bar{x}}\frac{u_1}{U_{N_s}}\right)\frac{\rho_1}{\rho_s}\right]^{1/2}\frac{B_1}{\sqrt{\lambda}} \tag{33}$$

where for a symmetrical cylinder with detached bow wave

$$\frac{\rho_s U_{N_s}}{\cos\beta} = \rho_\infty U_\infty$$

This latter relation would be only approximate for an asymmetrical cylinder.

Application to Stagnation Type of Flow

Initial values of λ and B_1.- In the vicinity of the stagnation line which occurs on a blunt leading edge for both the yawed and unyawed cylinder, u_1 approaches 0 as x approaches 0. Then, in order to avoid infinite values of $\frac{d\theta}{dx}$ and $\frac{d\varphi}{dx}$ at $x = 0$, the two following conditions, as obtained from equations (29) and (30), must be satisfied at $x = 0$:

$$2\frac{\theta}{\Delta} + \frac{\delta^*}{\Delta} + \frac{T_1^*}{T_{1_0}}\left(\frac{T_w}{T_1^*} - 1\right)\frac{\Delta^*}{\Delta} + \frac{263}{630}\left(\frac{T_1^*}{T_{1_0}} - 1\right) - \frac{T_w}{T_{1_0}}\frac{12 + \lambda}{6\lambda} = 0 \tag{34}$$

and

$$\frac{\varphi}{\Delta} - \frac{1}{\sigma}\frac{T_w}{T_{1_0}}\frac{B_1}{\lambda} = 0 \tag{35}$$

where equation (15) has been used to supply a relation between Δ^2, $\frac{du_1}{dx}$, and λ. The expressions for $\frac{\theta}{\Delta}$, $\frac{\delta^*}{\Delta}$, $\frac{\Delta^*}{\Delta}$, and $\frac{\varphi}{\Delta}$ are introduced into equations (34) and (35) from equations (22), (23), (26), and (27) with

B_2 and B_3 (from equations (20) and (21)) evaluated at $x = 0$. The parameter B_1 may then be eliminated between equations (34) and (35) and the following quadratic for $\frac{T_w}{T_{1_0}}$ results:

$$\left(\frac{4 - \lambda}{2\lambda}\right)\left(\frac{T_w}{T_{1_0}}\right)^2 + \left\{\sigma\lambda\left[\frac{\lambda - 4}{2\lambda}\left(\alpha_1 + \frac{\lambda}{6}\alpha_5\right) + \frac{1}{5}\left(\alpha_0 + \frac{\lambda}{6}\alpha_4\right)\right] - \left(2\frac{\theta}{\Delta} + \frac{\delta^*}{\Delta} - \frac{2}{3}\frac{T_1^*}{T_{1_0}}\right) - \left(\frac{T_1^*}{T_{1_0}} - 1\right)\left[\frac{263}{630} + \frac{4}{15}(1 - \sigma)\right]\right\}\frac{T_w}{T_{1_0}} - \frac{1}{5}\sigma\lambda\frac{T_1^*}{T_{1_0}}\left(\alpha_0 + \frac{\lambda}{6}\alpha_4\right) + \sigma\lambda\left(\alpha_1 + \frac{\lambda}{6}\alpha_5\right)\left\{\left(2\frac{\theta}{\Delta} + \frac{\delta^*}{\Delta} - \frac{2}{3}\frac{T_1^*}{T_{1_0}}\right) + \left(\frac{T_1^*}{T_{1_0}} - 1\right)\left[\frac{263}{630} + \frac{4}{15}(1 - \sigma)\right]\right\} - \frac{4}{5}\sigma\lambda(1 - \sigma)\left(\alpha_2 + \frac{\lambda}{6}\alpha_6\right)\left(\frac{T_1^*}{T_{1_0}} - 1\right) = 0 \tag{36}$$

where for $u_1 = 0$

$$\frac{T_1^*}{T_{1_0}} = 1 + \frac{v_1^2}{2c_pT_{1_0}} = \frac{1 + \frac{\gamma - 1}{2}M_\infty^2}{1 + \frac{\gamma - 1}{2}M_\infty^2 \cos^2 \beta} \tag{37}$$

since

$$v_1^2 = v_\infty^2 = \gamma RT_\infty M_\infty^2 \sin^2 \beta$$

and

$$\frac{T_1^*}{T_\infty} = 1 + \frac{\gamma - 1}{2} M_\infty^2$$

Then, for given values of M_∞ and β, equation (36) is solved for $\frac{T_w}{T_{1_0}}$ as a function of λ. Typical results for this calculation are shown in figure 1 for various values of T_1^*/T_{1_0}. The corresponding values of B_1 may be found from equation (35) as

$$B_1 = \frac{\alpha_0 + \frac{\lambda}{6}\alpha_4 + 4(1 - \sigma)\left(\alpha_2 + \frac{\lambda}{6}\alpha_6\right)\frac{T_1^* - T_{1_0}}{T_1^* - T_w}}{\frac{T_w}{T_{1_0}}\frac{1}{\sigma\lambda} - \left(\alpha_1 + \frac{\lambda}{6}\alpha_5\right)} \tag{38}$$

where equations (20), (21), and (27) evaluated at $x = 0$ have been used to obtain $\frac{\varphi}{\Delta}$.

Recovery temperature and heat-transfer coefficient at $x = 0$.- For the condition of zero heat transfer, $q_w = 0$ and the wall temperature T_w equals the recovery temperature T_e. Combining equations (38) and (32) and using these conditions give an expression for T_e which is

$$T_e = T_1^* + 4(1 - \sigma)\frac{\alpha_2 + \frac{\lambda}{6}\alpha_6}{\alpha_0 + \frac{\lambda}{6}\alpha_4}\left(T_1^* - T_{1_0}\right) \tag{39}$$

Then defining a recovery factor r in terms of the local temperature outside the boundary layer results in

$$r \equiv \frac{T_e - T_{1_0}}{T_1^* - T_{1_0}} = 1 + 4(1 - \sigma)\frac{\alpha_2 + \frac{\lambda}{6}\alpha_6}{\alpha_0 + \frac{\lambda}{6}\alpha_4} \tag{40}$$

which gives for values of σ near unity $r \approx \sqrt{\sigma}$ since equation (40) is almost independent of λ. (Actually, for zero heat transfer the value of λ must satisfy equations (39) and (36) with $T_w = T_e$.) This value of the recovery factor is in good agreement with the results of an exact analysis by Schuh (ref. 14).

A heat-transfer parameter using the conventional definition for the heat-transfer coefficient

$$h_c = \frac{q_w}{T_w - T_e} \tag{41}$$

may now be formed by substituting equations (38) and (39) into equation (33) so that

$$\frac{h_c L}{k_w \sqrt{\frac{\rho_\infty U_\infty L}{\mu_w}}} = \sqrt{\cos\beta\left(\frac{d}{d\bar{x}}\frac{u_1}{U_{N_s}}\right)\frac{\rho_{1_0}}{\rho_s}}\;\frac{\left(\alpha_0 + \frac{\lambda}{6}\alpha_4\right)(\lambda)^{-1/2}}{\frac{T_w}{T_{1_0}}\frac{1}{\sigma\lambda} - \left(\alpha_1 + \frac{\lambda}{6}\alpha_5\right)} \tag{42}$$

where all quantities are evaluated at $x = 0$. It may be noted that this relation is expected to apply in the vicinity of the stagnation line for an isothermal cylinder since $\left(\frac{d\lambda}{dx}\right)_{x=0} = 0$ and $\left(\frac{dB_1}{dx}\right)_{x=0} = 0$ as shown in the appendix and $\lim_{x \to 0} \frac{u_1}{x} = \left(\frac{du_1}{dx}\right)_{x=0}$. The function

$$F\left(\lambda, \frac{T_w}{T_{1_0}}\right) = \frac{\left(\alpha_0 + \frac{\lambda}{6}\alpha_4\right)(\lambda)^{-1/2}}{\frac{T_w}{T_{1_0}}\frac{1}{\sigma\lambda} - \left(\alpha_1 + \frac{\lambda}{6}\alpha_5\right)} \tag{43}$$

appearing in equation (42) has been computed with $\sigma = 0.7$ for a large range of T_1^*/T_{1_0} and the results are plotted against T_w/T_{1_0} in figure 2. This figure shows that, regardless of the values of M_∞ and β, the function F depends almost entirely on T_w/T_{1_0} where

$$\frac{T_w}{T_{1_0}} = \frac{T_w}{T_1^*} \frac{1 + \frac{\gamma - 1}{2} M_\infty^2}{1 + \frac{\gamma - 1}{2} M_\infty^2 \cos^2 \beta} \tag{44}$$

from equation (37). Thus, a numerical expression for F as a function of $\frac{T_w}{T_1^*}$, M_∞, and β could be used to give a universal correlation for the heat transfer along the stagnation line. Such an expression for $\sigma = 0.70$ is

$$F\left(\lambda, \frac{T_w}{T_{1_0}}\right) = 0.84\left(\frac{T_w}{T_{1_0}}\right)^{-0.3} - 0.4 \tag{45}$$

with a maximum error of about 4 percent for $2.5 > \frac{T_w}{T_{1_0}} > 0.10$. (See fig. 2.) The resulting correlation parameter from equations (42), (44) and (45) is then

$$\frac{h_c L}{k_w \sqrt{\frac{\rho_\infty U_\infty L}{\mu_w}}} = \sqrt{\cos \beta \frac{d}{d\bar{x}}\left(\frac{u_1}{U_{N_s}}\right) \frac{\rho_{1_0}}{\rho_s}} \left[0.84\left(\frac{T_w}{T_1^*} \frac{1 + \frac{\gamma - 1}{2} M_\infty^2}{1 + \frac{\gamma - 1}{2} M_\infty^2 \cos^2 \beta}\right)^{-0.3} - 0.4\right] \tag{46}$$

which is a function of the yaw angle β, the stream Mach number M_∞, and the wall-to-stagnation-temperature ratio T_w/T_1^*. The quantity ρ_{1_0}/ρ_s depends on the chordwise component of the Mach number just behind the shock $\left(M_{N_s}\right)$ according to the isentropic relation

$$\frac{\rho_{1_0}}{\rho_s} = \left(1 + \frac{\gamma - 1}{2} M_{N_s}^{\ 2}\right)^{\frac{1}{\gamma-1}} \tag{47}$$

It should be noted at this point that by analogy with the results of reference 11 equation (46) is expected to underestimate the heat transfer coefficient by as much as 10 to 30 percent when $T_w > T_e$ (see fig. 3, ref. 11).

Application to a circular cylinder.- The velocity-gradient parameter in equation (46) is evaluated from a modified Newtonian type pressure coefficient (ref. 15) which is written for a circular cylinder as

$$C_p = \frac{p_1 - p_\infty}{\frac{1}{2}\rho_\infty u_\infty^{\ 2}} = \frac{p_{1_0} - p_\infty}{\frac{1}{2}\rho_\infty u_\infty^{\ 2}} \cos^2\left(2\frac{x}{D}\right)$$

where D is the cylinder diameter. This equation modifies the usual expression for the Newtonian pressure coefficient (ref. 16) so that the correct pressure coefficient is obtained at the stagnation line. An analogous equation may be easily derived for any other cross-sectional shape. Differentiating the equation for a circular cylinder twice with respect to x and evaluating at $x = 0$ give

$$\frac{d^2p_1}{d\bar{x}^2} = -8\left(p_{1_0} - p_\infty\right) \tag{48}$$

Bernoulli's equation (8) requires that

$$\lim_{x \to 0}\left(\frac{du_1}{d\bar{x}}\right) = \left[-\frac{1}{\rho_{1_0}} \frac{d^2p_1}{d\bar{x}^2}\right]_{x=0}^{1/2} \tag{49}$$

hence, from equation (48),

$$\left(\frac{du_1}{d\bar{x}}\right)_{x=0} = \left[8\frac{p_{1_0} - p_\infty}{\rho_{1_0}}\right]^{1/2}$$

or introducing the chordwise velocity U_{N_s} behind the shock gives

$$\left(\frac{d}{d\bar{x}}\frac{u_1}{U_{N_s}}\right)_{x=0} = \left[8\left(1 - \frac{p_\infty}{p_{1_0}}\right)\frac{\frac{T_{1_0}}{T_s}}{\gamma M_{N_s}^{\ 2}}\right]^{1/2} \tag{50}$$

This relation has been plotted against the crossflow Mach number $M_{N_\infty} = M_\infty \cos \beta$ in figure 3 where it is compared with some experimental results on cylinders. The experimental values shown are the results of some previously unpublished data obtained in the Gas Dynamic Branch of the Langley Laboratory. The length of the vertical line through the data points corresponds to the maximum experimental error.

Chordwise velocity profile at the stagnation line for zero heat transfer.- As an indication of the accuracy of the present method for the condition of zero heat transfer, the chordwise velocity profile at $x = 0$ is compared with the results of Crabtree's linearized solution of the same problem (ref. 8). The chordwise profile given by equation (14) is transformed back to the z-plane by means of the relation

$$z\sqrt{\frac{1}{\lambda\nu_{1_0}}\frac{du_1}{dx}\frac{T_{1_0}}{T_1{}^*}} = \int_0^{\eta^*}\frac{\rho_1{}^*}{\rho}\,d\eta^* \tag{51}$$

which is the inverse of equation (10) combined with the expression for Δ from equation (15) evaluated for $T_w = T_1{}^*$ and $\frac{\mu_1{}^*}{\mu_{1_0}} = \frac{T_1{}^*}{T_{1_0}}$ corresponding to the conditions of zero heat transfer, $\sigma = 1$, and the viscosity-temperature relation of reference 8. The density ratio in the above equation, for these conditions, is written as

$$\frac{\rho_1^*}{\rho} = \frac{\rho_1^*}{\rho_{1_0}}\left\{\frac{T_1^*}{T_{1_0}} - \left(\frac{T_1^*}{T_{1_0}} - 1\right)\left[4(\eta^*)^2 - 8(\eta^*)^4 + 4(\eta^*)^5 + 4(\eta^*)^6 - 4(\eta^*)^7 + (\eta^*)^8\right]\right\}$$

from the definitions of H and $\bar{t}$ and equations (4), (9), (17), and (37). Inserting this density ratio in the first equation and integrating gives the final required relation between z and η^*. The value of λ required in equations (14) and (51) was obtained from equation (36) for these same conditions and is 7.249.

The results of this calculation for a spanwise Mach number of unity are shown in figure 4 where u/u_1 is plotted against the distance parameter $\left(\frac{du_1}{dx}\frac{1}{\nu_{1_0}}\right)^{1/2} z$. The reasonable agreement between the present method and Crabtree's more exact analysis indicates that the compressibility effects, in this particular case, are predicted satisfactorily by the approximate integral solution.

COMPARISON OF THEORY WITH EXPERIMENTAL DATA

The experimental data of reference 3 are representative of an average heat-transfer rate per unit area or, alternately, the total heat-transfer rate for the forward half of a circular cylinder. A dimensionless parameter of the form $\frac{\bar{h}_c D}{k_s\sqrt{\frac{\rho_\infty U_\infty D}{\mu_s}}}$ was found to correlate the data for all yaw angles as shown in reference 3. The theoretical analysis applied to the local heat-transfer coefficient at the stagnation line yields for this same parameter the expression

$$\frac{h_c D}{k_s\sqrt{\frac{\rho_\infty U_\infty D}{\mu_s}}} = \sqrt{\frac{\mu_w}{\mu_s}\cos\beta\,\frac{d}{d\bar{x}}\left(\frac{u_1}{U_{N_s}}\right)\frac{\rho_{1_0}}{\rho_s}}\left[0.84\left(\frac{T_w}{T_1^*}\,\frac{1 + \frac{\gamma - 1}{2}M_\infty^2}{1 + \frac{\gamma - 1}{2}M_\infty^2\cos^2\beta}\right)^{-0.3} - 0.4\right] \tag{52}$$

from equation (46) with $k_w = \frac{\mu_w}{\mu_s} k_s$ (c_p and σ being assumed constant) and $\bar{x} = \frac{x}{D}$. This has been plotted in the lower part of figure 5 for $M_\infty = 6.9$, $T_1{}^* = 1200^\circ$ R and $\frac{T_w}{T_1{}^*} = 0.2, 0.5, 0.8$, corresponding approximately to the experimental test conditions $\left(\text{except for } \frac{T_w}{T_1{}^*} = 0.2\right)$. Comparison of the theory with the data indicates that the measured effect of yaw on the average or total heat transfer on a half-cylinder is considerably less than the theoretically predicted effect on the local heat transfer in the vicinity of the stagnation line. Thus, in order to obtain a more complete comparison of the theory with experiment, it is necessary to calculate from the theory the local heat transfer over the entire half-cylinder. This calculation was carried out (according to a general procedure outlined in the appendix) for two angles of yaw, $\beta = 0^\circ$ and $\beta = 60^\circ$, with $M_\infty = 6.9$, $dT_w/dx = 0$, $\frac{T_w}{T_1{}^*} = 0.5$ and 0.2, and $T_1{}^* = 1200^\circ$ R.

The values of M_1 and $\frac{dM_1}{d\bar{x}}$ required in the calculation were obtained from the faired curves shown in figure 6. These curves are based on the experimental data included in this figure as well as values of $\left(\frac{dM_1}{d\bar{x}}\right)_{x=0}$ computed from the data shown in figure 3. The data points shown in figure 6 were computed directly from measured pressure data according to the isentropic relation

$$M_1{}^2 = \frac{2}{\gamma - 1}\left[\left(\frac{p_{1_0}}{p_1}\right)^{\frac{\gamma-1}{\gamma}} - 1\right]$$

which, from inviscid theory for yawed infinite cylinders, would depend only on the value of M_{N_∞}. Consequently, since some of the data from reference 15 show considerable scatter, some additional data (previously unpublished) at a comparable M_{N_∞} have been included. Then largely on the basis of these data for $M_{N_\infty} = 4.08$ and the results of figure (3), the erratic data for $0.5 > \bar{x} > 0$ could be overlooked and the curves shown result.

The results of the calculation are shown in figure 7 where the ratio $q_w/\left(q_w\right)_{x=0}$ is plotted against $\bar{x}$ for the two yaw angles and temperature ratios considered. Note that the variation of $q_w/\left(q_w\right)_{x=0}$ with yaw angle and temperature ratio is not very large and, for practical purposes, could be considered a function of $\bar{x}$ only. Also included in figure 7 are the initial values of the basic theoretical parameter $\dfrac{q_w D}{k_w\left(T_w - T_1{}^*\right)\sqrt{\dfrac{\rho_\infty U_\infty D}{\mu_w}}}$ from equation (33). The present method fails for $\lambda > 12$ (see appendix) which occurred in all cases before $\bar{x} = \frac{\pi}{4}$ as indicated in figure 7. However, sufficient information was obtained to permit a reasonable extrapolation to $\bar{x} = \frac{\pi}{4}$ which was used as the basis for the following calculations.

The average heat-transfer coefficient $\bar{h}_c$ was obtained by integration over $\bar{x}$ of the local computed values of q_w and then division by $\left(T_w - T_e\right)\bar{x}$ where T_e was taken as the experimental value according to the upper part of figure 5. These average heat-transfer coefficients were then used to compute the values of the parameter $\dfrac{\bar{h}_c D}{k_\infty}\sqrt{\dfrac{\mu_\infty}{\rho_\infty U_\infty D}}$ which are shown in figure 8. (Accurate values of μ_w/μ_∞ and k_w/k_∞ were used in computing this parameter). The experimental data in the form of this same parameter (ref. 3) are also plotted in figure 8. Comparison of the theoretical values with the experimental data reveals that the predicted heat transfer is about 40 percent less than the experimental results for a yaw angle of 60° whereas at a yaw angle of 0° the agreement is good. The reasons for the discrepancy at large yaw angles are not yet clear; however, at least part of the difference may be due to the configuration of the test model used in reference 3. The finite length and end shape would both tend to make the test cylinder approximate something between an infinite yawed cylinder and a pointed body of revolution at angle of attack so that the measured heat transfer could possibly depend on the distance from the end as well as the yaw angle. Actually, in view of the approximating assumptions involved in the theory (mainly, the universal boundary-layer thickness and the linear viscosity relation) and the possibility of certain indeterminate factors in the experiment (such as end conditions and spanwise heat conduction), the agreement between theory and experiment is probably as good as can be expected.

On the basis of the results of the present method at the stagnation line (eq. 40) and Schuh's theoretical results (ref. 14), the value of a

"local" recovery factor would be

$$r = \frac{T_e - T_1}{T_1^* - T_1} = \sqrt{\sigma} \tag{53}$$

This assumption cannot be compared directly with the experimental values of reference 3 which represent an average recovery factor or equilibrium temperature for the condition of zero total heat input to the entire half-cylinder. However, an average equilibrium temperature may be defined and evaluated from equation (53) with the result that

$$\left(\frac{T_e}{T_1^*}\right)_{av} = \sqrt{\sigma} + (1 - \sqrt{\sigma})\frac{1 + \frac{\gamma - 1}{2}M_\infty^2 \cos^2 \beta}{1 + \frac{\gamma - 1}{2}M_\infty^2}\frac{4}{\pi}\int_0^{\frac{\pi}{4}} \frac{T_1}{T_{1_0}}\, d\bar{x} \tag{54}$$

where equation (37) has been used and T_1/T_{1_0} depends only on M_1 from figure 6. This average T_e/T_1^*, which is a function of the yaw angle only for a given M_∞, is compared with the experimental values in the upper part of figure 5. Although exact agreement between theory and experiment is not expected since the local heat transfer is not everywhere zero in the experiment, the use of equation (53) is confirmed in this case.

CONCLUSIONS

An integral method has been developed for the calculation of the compressible laminar boundary layer on yawed infinite cylinders of arbitrary shape and with arbitrary wall temperature distribution. In general, the method requires the numerical solution of two simultaneous ordinary first-order differential equations. At the stagnation line of a blunt cylinder the solution reduces to a set of algebraic equations which result in a general correlation equation for the heat transfer in the vicinity of the stagnation line. An expression is also derived for the recovery factor which is in good agreement with an exact solution and some experimental data. The chordwise velocity profile at the stagnation line as computed from the present method for zero heat transfer and a Prandtl number of unity is also in good agreement with a more exact solution.

The method is applied to the calculation of local heat-transfer rates on the front part of a circular cylinder at a stream Mach number of 6.9 and angles of yaw of 0° and 60°. The results of this calculation indicate that the variation in local heat transfer around the surface of the cylinder has very little functional dependence on yaw angle or wall temperature. Comparison of the calculations with some experimental data, which shows the effect of yaw on the average heat transfer to a simulated leading edge, gives good agreement at small yaw angles but at a yaw angle of 60° the theoretical heat transfer is about 40 percent less than the measured value. This discrepancy may be caused partly by indeterminate factors in the data as well as the simplifying assumptions involved in the theory.

Langley Aeronautical Laboratory,
National Advisory Committee for Aeronautics,
Langley Field, Va., June 7, 1955.

APPENDIX

CALCULATION PROCEDURE

General Method

Equations (29) and (30) are written in the form

$$\frac{dZ}{d\bar{x}} + 2Z\left\{2 + \frac{\gamma - 1}{2}M_1^2 + \left(1 + \frac{\gamma - 1}{2}M_1^2\right)\frac{\delta^*}{\theta} + \frac{T_1^*}{T_1}\left(\frac{T_w}{T_1^*} - 1\right)\frac{\Delta^*}{\theta} + \frac{263}{630}\frac{\theta}{\Delta}\left[\frac{T_1^*}{T_1} - \left(1 + \frac{\gamma - 1}{2}M_1^2\right)\right]\right\}\frac{1}{u_1}\frac{du_1}{d\bar{x}} = 2\frac{\rho_w}{\rho_1^*}\frac{\mu_w}{u_1\rho_1^* L}R_{s_L}\frac{12 + \lambda}{6}\frac{\theta}{\Delta} \tag{A1}$$

and

$$\frac{d\phi}{d\bar{x}} + 2\phi\left(\frac{1}{u_1}\frac{du_1}{d\bar{x}} - \frac{c_p}{t_1^*}\frac{dT_w}{d\bar{x}}\right) = \frac{2}{\sigma}\frac{\rho_w}{\rho_1^*}\frac{\mu_w}{u_1\rho_1^* L}R_{s_L}B_1\frac{\varphi}{\Delta} \tag{A2}$$

where the parameters Z and ϕ have been introduced so as to avoid the use of the second velocity derivative $\frac{d^2u_1}{dx^2}$ which is difficult to obtain accurately from experimental data. The quantity R_{s_L} is the Reynolds number at some reference point, for example, just behind the bow shock on a blunt cylinder. The computing parameters are defined as

$$Z \equiv R_{s_L}\left(\frac{\theta}{L}\right)^2 = \left(\frac{\rho_w}{\rho_1^*}\right)^2\frac{\mu_w}{\rho_1 L}\frac{R_{s_L}}{\frac{du_1}{d\bar{x}}}\lambda\left(\frac{\theta}{\Delta}\right)^2 \tag{A3}$$

and

$$\phi \equiv R_{s_L}\left(\frac{\varphi}{L}\right)^2 = \left(\frac{\rho_w}{\rho_1^*}\right)^2 \frac{\mu_w}{\rho_1 L} \frac{R_{s_L}}{\frac{du_1}{d\bar{x}}} \lambda \left(\frac{\varphi}{\Delta}\right)^2 \tag{A4}$$

where equation (15) has been used to provide the relation between λ and Δ. For convenience, all quantities needed for the solution of these equations are listed below:

$$\frac{\theta}{\Delta} = \frac{1}{315}\left(37 - \frac{\lambda}{3} - \frac{5\lambda^2}{144}\right) \tag{22}$$

$$\frac{\delta^*}{\Delta} = \frac{36 - \lambda}{120} \tag{23}$$

$$\frac{\Delta^*}{\Delta} = \frac{2}{3} - \frac{1}{5}B_1 - \frac{1}{15}B_2 - \frac{1}{60}B_3 \tag{26}$$

$$\frac{\varphi}{\Delta} = \alpha_0 + \frac{\lambda}{6}\alpha_4 + \left(\alpha_1 + \frac{\lambda}{6}\alpha_5\right)B_1 + \left(\alpha_2 + \frac{\lambda}{6}\alpha_6\right)B_2 + \left(\alpha_3 + \frac{\lambda}{6}\alpha_7\right)B_3 \tag{27}$$

$$B_2 = (1 - \sigma)\frac{T_1}{T_1^* - T_w}\left\{4\left(\frac{T_1^*}{T_1} - 1\right) + \frac{\gamma - 1}{2}M_1^2\left[\left(\frac{12 + \lambda}{6}\right)^2 - 4\right]\right\} \tag{A5}$$

$$B_3 = \frac{\gamma - 1}{2}M_1^2\frac{T_1}{T_1^* - T_w}\frac{12\lambda + \lambda^2}{6}\left(\sigma - 1 + \frac{\sigma c_p}{3u_1}\frac{T_1}{T_w}\frac{\frac{dT_w}{d\bar{x}}}{\frac{du_1}{d\bar{x}}}\right) \tag{A6}$$

$$\frac{T_1^*}{T_1} \equiv \frac{T_{1_0}}{T_1}\frac{T_1^*}{T_{1_0}} = \left(1 + \frac{\gamma - 1}{2}M_1^2\right)\frac{1 + \frac{\gamma - 1}{2}M_\infty^2}{1 + \frac{\gamma - 1}{2}M_\infty^2 \cos^2 \beta} \tag{A7}$$

where equation (37) has been used in the last expression. Equations (A5) and (A6) are obtained from equations (20) and (21) with equation (31) used where necessary. The simultaneous solution of equations (A1), (A2), (A3), and (A4) for Z, λ, ϕ, and B_1 can now be carried out by any suitable graphical or numerical procedure. The values of u_1 $\left(\text{or } M_1\right)$, T_w, T_1^*, M_∞, and β must be given. A typical numerical procedure is applied to the same type of problem in reference 12.

Initial Values

Blunt leading edge.- In order to start the integration the values at $x = 0$ of Z, λ, ϕ, B_1, and their first derivatives must be known. For a blunt cylinder the initial values of λ and B_1 are obtained from equation (36) (or fig. 1) and equation (38). The corresponding values of Z and ϕ may then be obtained from equations (A3) and (A4). For the condition that $\frac{d\theta}{dx}$ and $\frac{d\varphi}{dx}$ are finite at $x = 0$ on a blunt cylinder, it can be shown from equations (29) and (30) that $\left(\frac{d\Delta}{dx}\right)_{x=0} = 0$ and $\left(\frac{dB_1}{dx}\right)_{x=0} = 0$ provided that $\left(\frac{d^2u_1}{dx^2}\right)_{x=0} = 0$ and $\left(\frac{dT_w}{dx}\right)_{x=0} = 0$. Then from equations (A3) and (A4), it follows that $\left(\frac{dZ}{dx}\right)_{x=0} = 0$ and $\left(\frac{d\phi}{dx}\right)_{x=0} = 0$.

Sharp leading edge with $\frac{du_1}{dx} \neq 0$.- At a sharp leading edge $\Delta = 0$ which requires that $(\lambda)_{x=0} = 0$ from equation (15). Hence $(Z)_{x=0} = 0$ and $(\phi)_{x=0} = 0$ from equations (A3) and (A4).

Substitution of the values of Δ and $d\Delta/dx$ from equation (15) into equation (29) and setting $\lambda = 0$ result in

$$\left(\frac{d\lambda}{d\bar{x}}\right)_{x=0} = \frac{1260}{37}\left(\frac{T_w}{T_1}\frac{1}{u_1}\frac{du_1}{d\bar{x}}\right)_{x=0} \tag{A8}$$

The required expression for $\left(\frac{dZ}{d\bar{x}}\right)_{x=0}$ is then obtained from equation (A3) after using equation (15), setting $\lambda = 0$, and inserting equation (A8) which gives

$$\left(\frac{dZ}{d\bar{x}}\right)_{x=0} = \frac{148}{315}\frac{(\mu_w\rho_w)_{x=0}}{\mu_1{}^*\rho_1{}^*} \tag{A9}$$

where for a sharp leading edge the quantity R_{s_L} would be designated as $\frac{\rho_1{}^*L}{\mu_1{}^*}\left(u_1\right)_{x=0}$.

The initial value of B_1 is obtained as

$$B_1 = \frac{630\sigma}{37 - 630\sigma\alpha_1}\left[\alpha_0 + 4\alpha_2(1 - \sigma)\frac{T_1{}^* - T_1}{T_1{}^* - T_w}\right]_{x=0} \tag{A10}$$

by substituting the values of Δ and $d\Delta/dx$ from equation (15) and φ/Δ from equation (27) into equation (30) and setting $\lambda = 0$. The required values of B_2 and B_3 are evaluated from equations (A5) and (A6) with $\lambda = 0$. It is of interest to note that, for $q_w = 0$, $B_1 = 0$ from equation (33), and then equation (A10) reduces to equation (40) with $\lambda = 0$.

The initial value of $\frac{d\phi}{d\bar{x}}$ is obtained by using the derivative of equation (15) in the derivative of equation (A4) and setting $\lambda = 0$. The result is

$$\left(\frac{d\phi}{d\bar{x}}\right)_{x=0} = \frac{37}{315}\left[\frac{\mu_w\rho_w}{\mu_1{}^*\rho_1{}^*}\left(\frac{B_1}{\sigma}\right)^2\right]_{x=0}$$

after using equations (A8) and (A10). The expression for $\left(\frac{dB_1}{d\bar{x}}\right)_{x=0}$ is too lengthy to include here, particularly since this expression, although convenient, is not essential to the integration procedure.

Sample Problem

The present method is applied to the calculation of local heat-transfer rates on a circular cylinder at a stream Mach number of 6.9, $\frac{dT_w}{dx} = 0$, $\beta = 0^\circ$ and 60°, and $\frac{T_w}{T_1{}^*} = 0.2$ and 0.5. Typical results of this calculation are shown in figure 9 where Z, λ, ϕ, and B_1 are plotted against $\bar{x}$. Note that in all cases λ goes to 12 at some value of $\bar{x} < \frac{\pi}{4}$ $\left(\bar{x} = \frac{\pi}{4}\right.$ corresponds to 90° back on the cylinder$\left.\right)$ as shown in figure 9(a). The calculation breaks down for $\lambda > 12$ because of the incompatible values of Z and $\frac{dZ}{d\bar{x}}$ required to satisfy equations (A3) and (A1) for $\lambda > 12$. The physical reason for this is that the local chordwise velocity within the boundary layer tends to exceed the external chordwise velocity due to the large values of $\frac{du_1}{dx}$ and $\frac{T_w}{T_1}$. A similar phenomena has been observed in certain exact solutions of wedge-type flows (ref. 17).

REFERENCES

1. Sears, W. R.: The Boundary Layer of Yawed Cylinders. Jour. Aero. Sci., vol. 15, no. 1, Jan. 1948, pp. 49-52.

2. Goland, Leonard: A Theoretical Investigation of Heat Transfer in the Laminar Flow Regions of Airfoils. Jour. Aero. Sci., vol. 17, no. 7, July 1950, pp. 436-440.

3. Feller, William V.: Investigation of Equilibrium Temperatures and Average Laminar Heat-Transfer Coefficients for the Front Half of Swept Circular Cylinders at a Mach Number of 6.9. NACA RM L55F08a, 1955.

4. Eggers, A. J., Jr., Hansen, C. Frederick, and Cunningham, Bernard E.: Theoretical and Experimental Investigation of the Effect of Yaw on Heat Transfer to Circular Cylinders in Hypersonic Flow. NACA RM A55E02, 1955.

5. King, Louis Vessot: On the Convection of Heat From Small Cylinders in a Stream of Fluid: Determination of Convection Constants of Small Platinum Wires With Applications to Hot-Wire Anemometry. Phil. Trans. Roy. Soc. (London), ser. A, vol. 214, Nov. 12, 1914, pp. 373-432, especially p. 402.

6. Struminsky, V. V.: Sideslip in a Viscous Compressible Gas. NACA TM 1276, 1951.

7. Moore, Franklin K.: Three-Dimensional Compressible Laminar Boundary-Layer Flow. NACA TN 2279, 1951.

8. Crabtree, L. F.: The Compressible Laminar Boundary Layer on a Yawed Infinite Wing. Aero. Quarterly, vol. V, pt 2, July 1954, pp. 85-100.

9. Kalikhman, L. E.: Heat Transmission in the Boundary Layer. NACA TM 1229, 1949.

10. Libby, Paul A., and Morduchow, Morris: Method for Calculation of Compressible Laminar Boundary Layer With Axial Pressure Gradient and Heat Transfer. NACA TN 3157, 1954.

11. Beckwith, Ivan E.: Heat Transfer and Skin Friction by an Integral Method in the Compressible Laminar Boundary Layer with a Streamwise Pressure Gradient. NACA TN 3005, 1953.

12. Morris, Deane N., and Smith, John W.: The Compressible Laminar Boundary Layer With Arbitrary Pressure and Surface Temperature Gradients. Jour. Aero. Sci., vol. 20, no. 12, Dec. 1953, pp. 805-818.

13. Tetervin, Neal: Boundary-Layer Momentum Equations for Three-Dimensional Flow. NACA TN 1479, 1947.

14. Schuh, H.: Aerodynamic Heating on Yawed Infinite Wings and on Bodies of Arbitrary Shape. KTH Aero Tn 35, Roy. Inst. of Tech., Div. of Aero. (Stockholm, Sweden), 1953.

15. Penland, Jim A.: Aerodynamic Characteristics of a Circular Cylinder at Mach Number 6.86 and Angles of Attack Up to 90°. NACA RM L54A14, 1954.

16. Grimminger, G., Williams, E. P., and Young, G. B. W.: Lift on Inclined Bodies of Revolution in Hypersonic Flow. Jour. Aero. Sci., vol. 17, no. 11, Nov. 1950, pp. 675-690.

17. Brown, W. Byron, and Donoughe, Patrick L.: Tables of Exact Laminar-Boundary-Layer Solutions When the Wall is Porous and Fluid Properties Are Variable. NACA TN 2479, 1951.

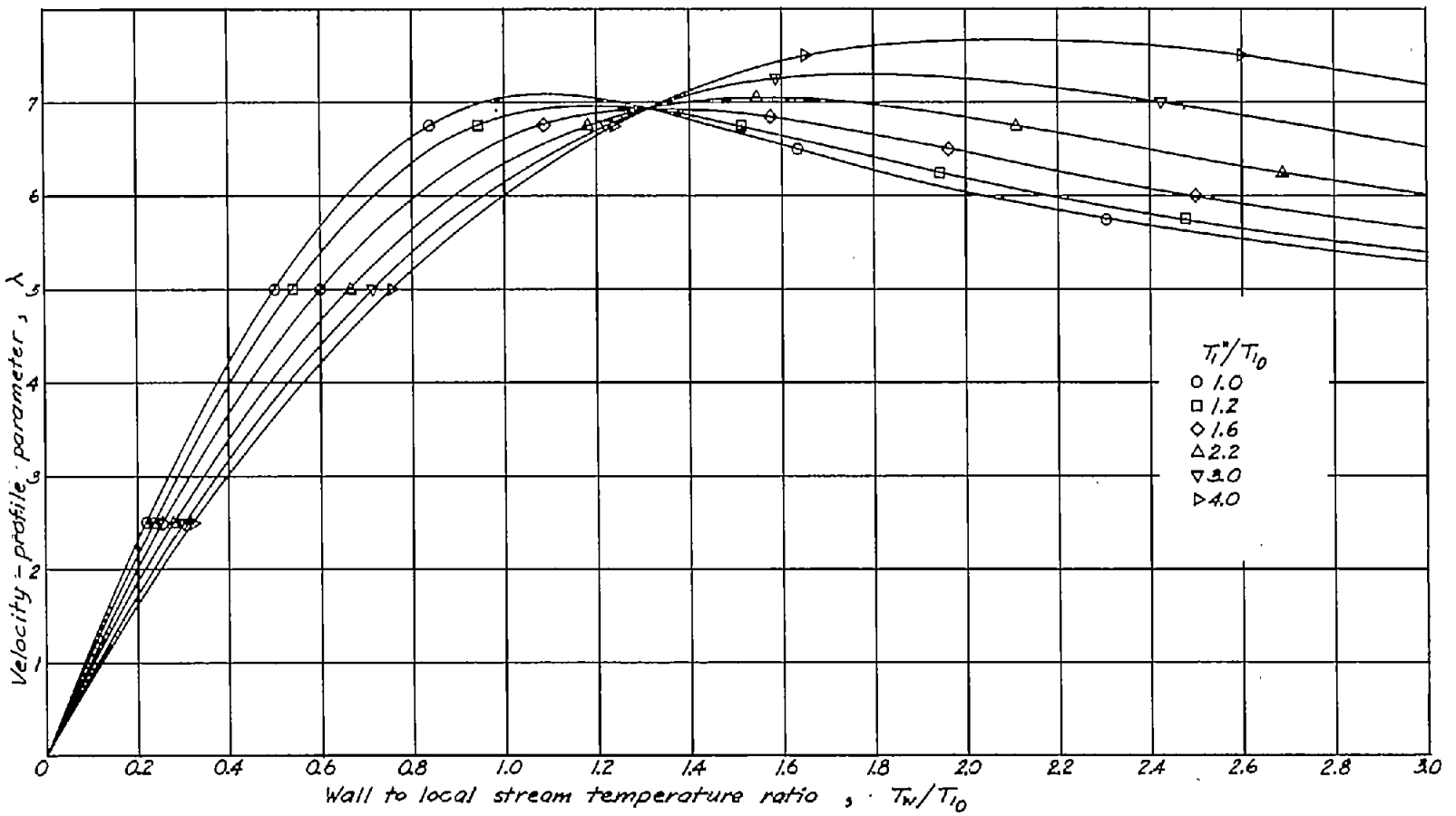

Figure 1.- The variation of λ with T_w/T_{1_0} (from eq. (36)) at the stagnation line for different values of T_1^*/T_{1_0} ($\sigma = 0.70$).

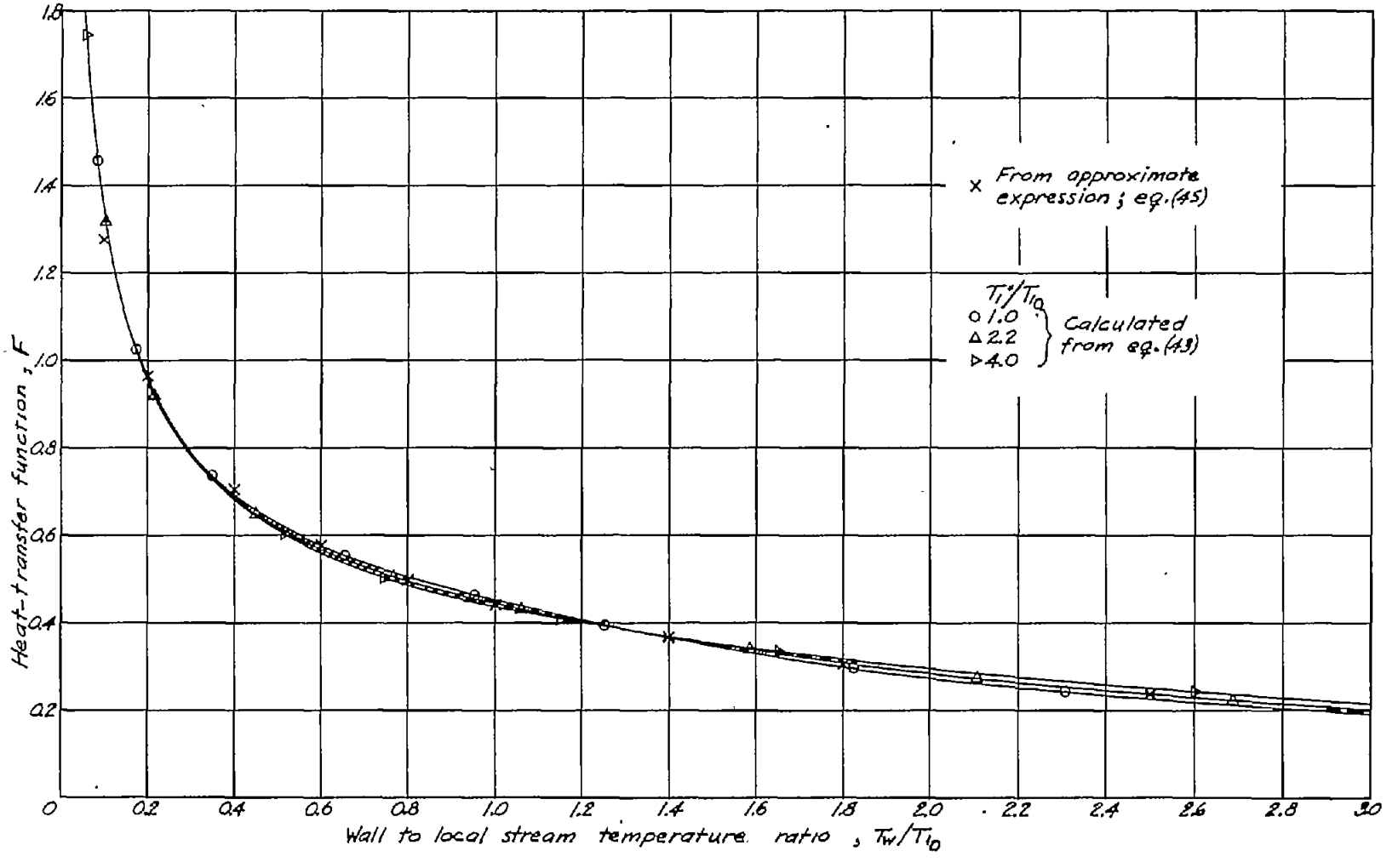

Figure 2.- Comparison of the calculated and approximate variation of F with T_w/T_{1_0} (σ = 0.70).

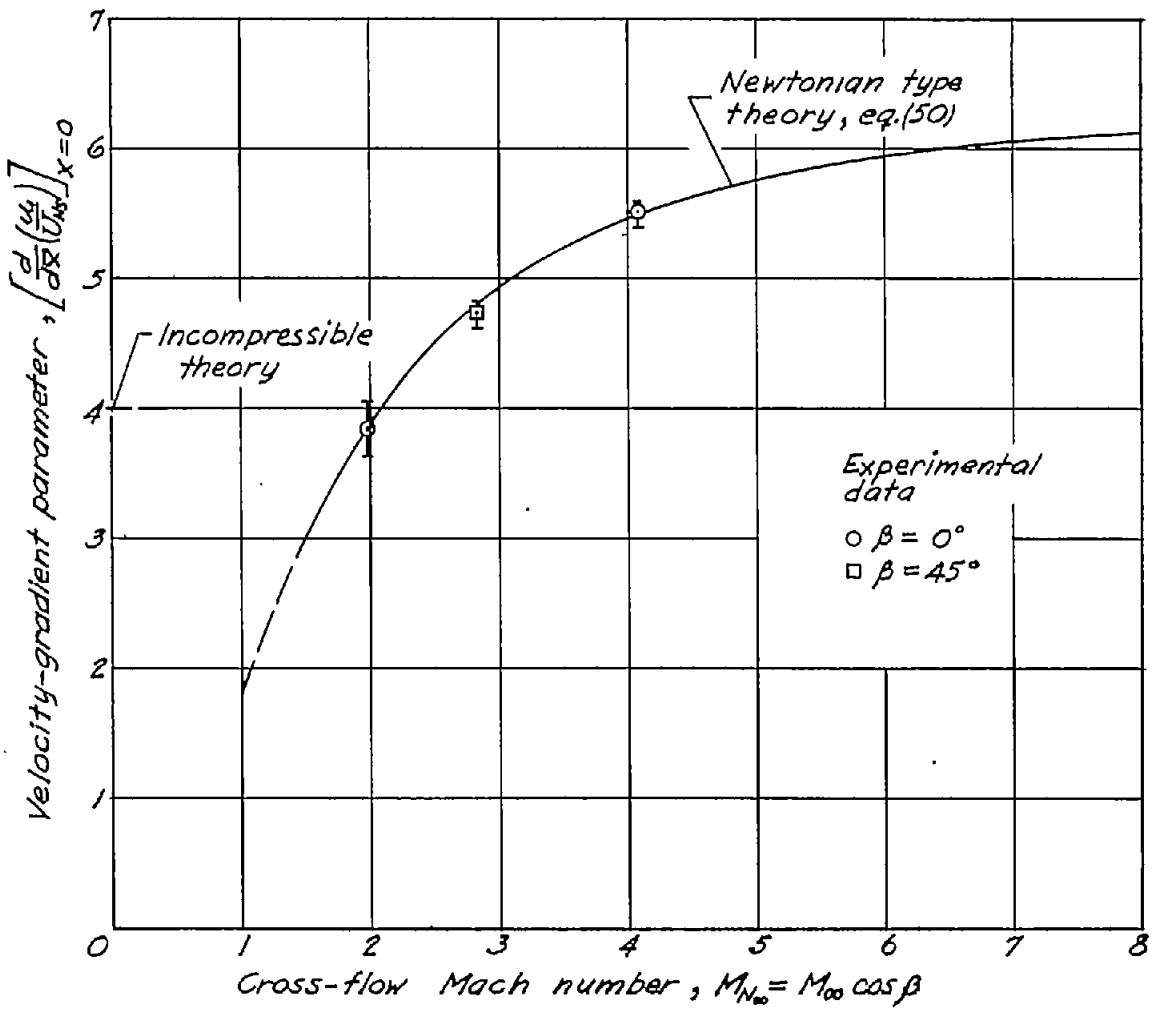

Figure 3.- Comparison of experimental and theoretical values of velocity-gradient parameter at the stagnation line of a circular cylinder.

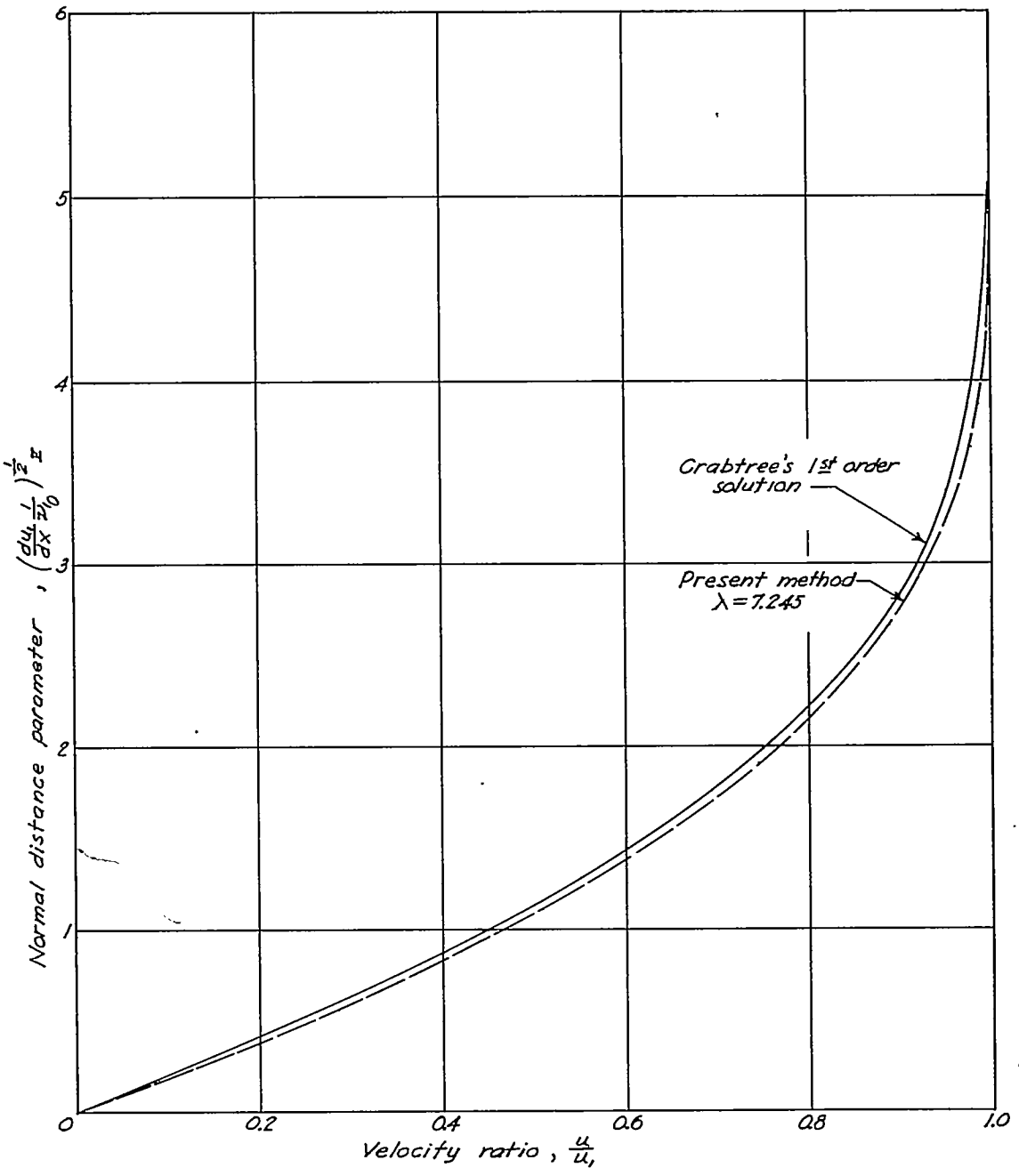

Figure 4.- Chordwise velocity profiles at the stagnation line as obtained from the present method and as given by Crabtree (ref. 8). Both curves are for the conditions of zero heat transfer, Prandtl number unity, and spanwise Mach number unity or $T_1^*/T_{1_0} = 1.2$, and $\rho_{1_0}/\rho_1^* = 0.634$.

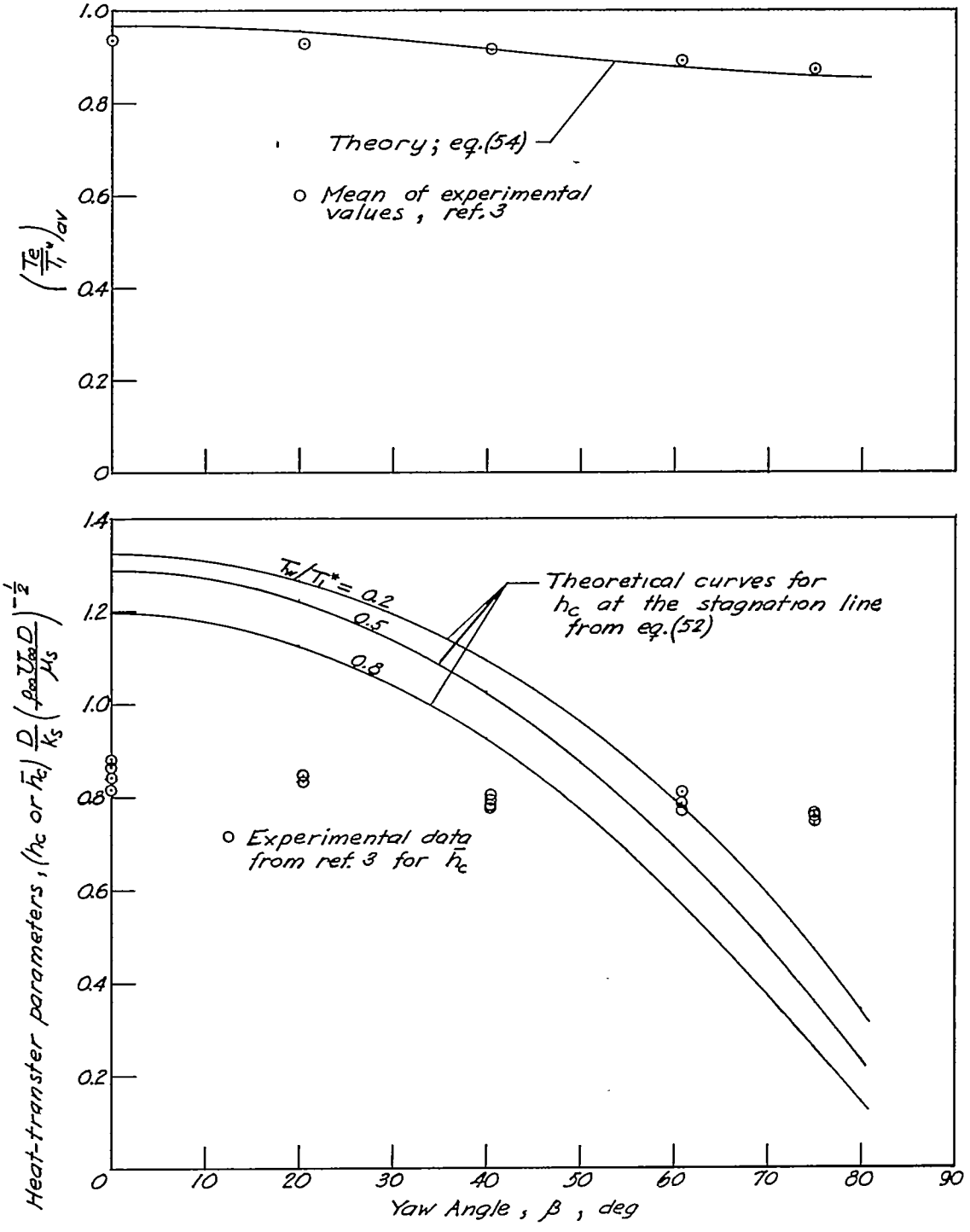

Figure 5.- Theoretical and experimental variation of heat transfer and recovery temperature with yaw angle on a circular cylinder at $M_\infty = 6.9$ and $T_1^* = 1200^\circ$ R.

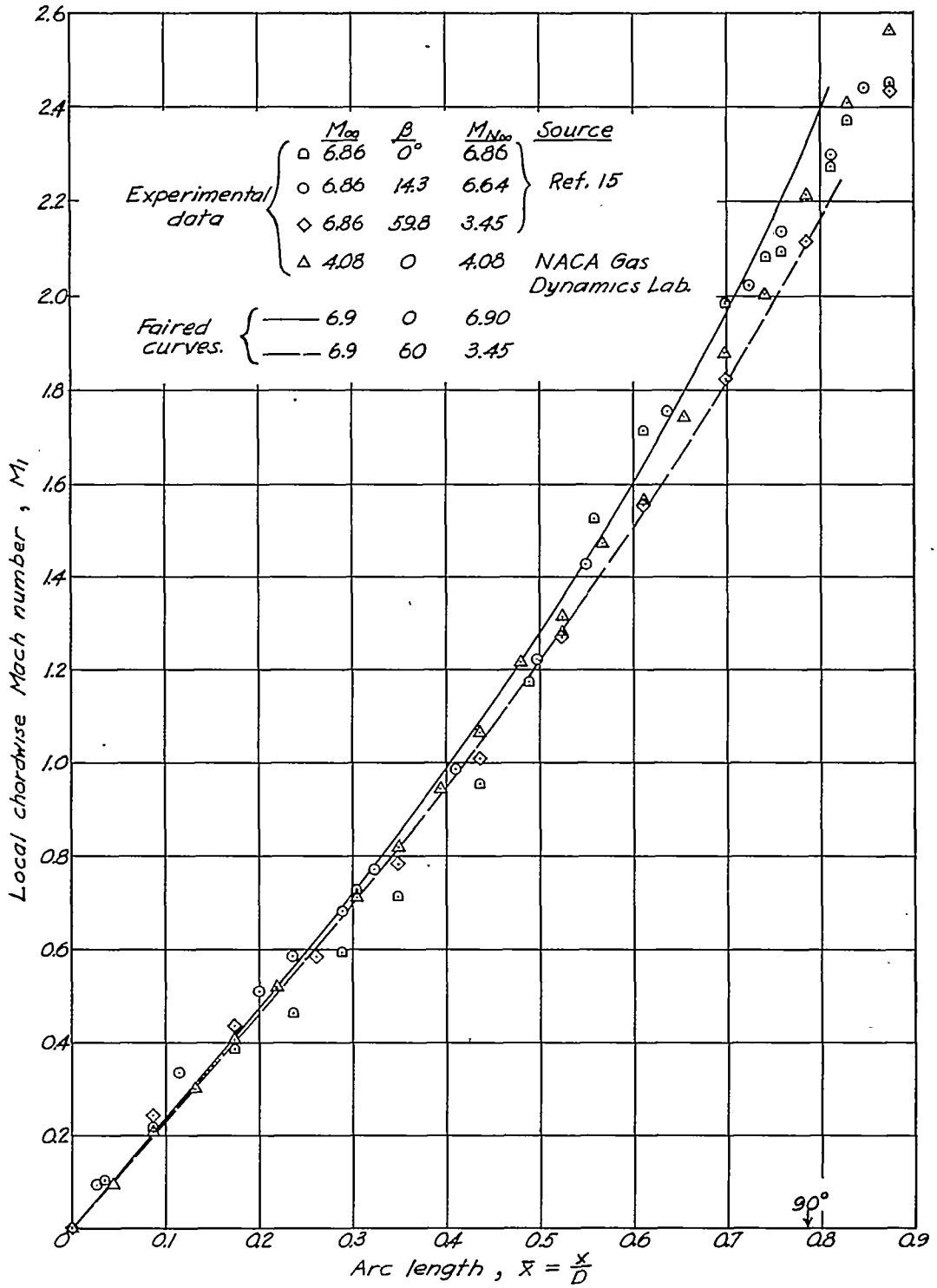

Figure 6.- Chordwise Mach number distribution on yawed and unyawed circular cylinders. The initial slope of the faired curves was computed from figure 3. These faired curves were used in the theoretical calculations.

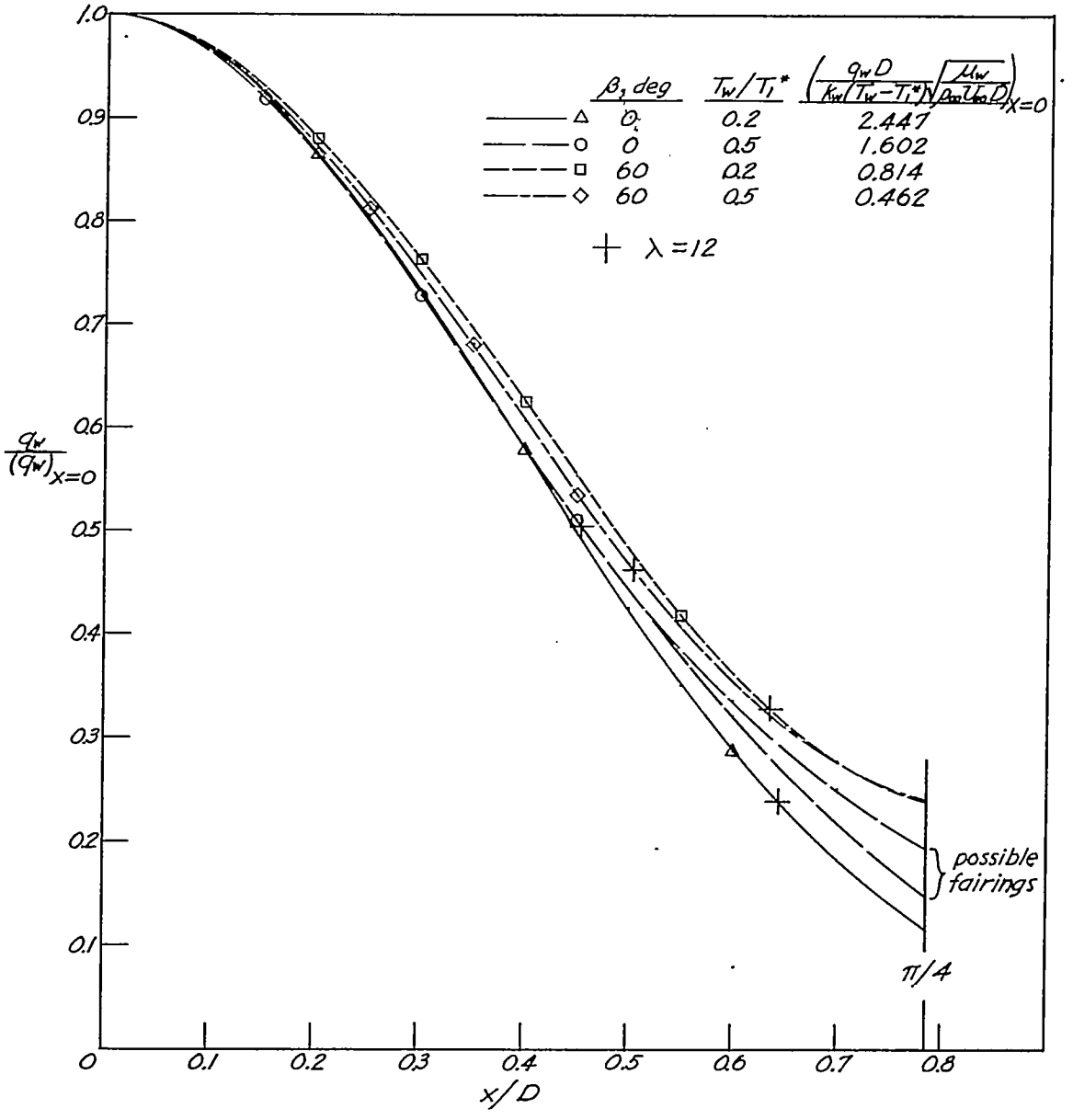

Figure 7.- The ratio of the calculated local heat transfer to the value at $x = 0$ on a circular cylinder at yaw angles of 0° and 60° for $M_\infty = 6.9$ and $T_1^* = 1200^\circ$ R.

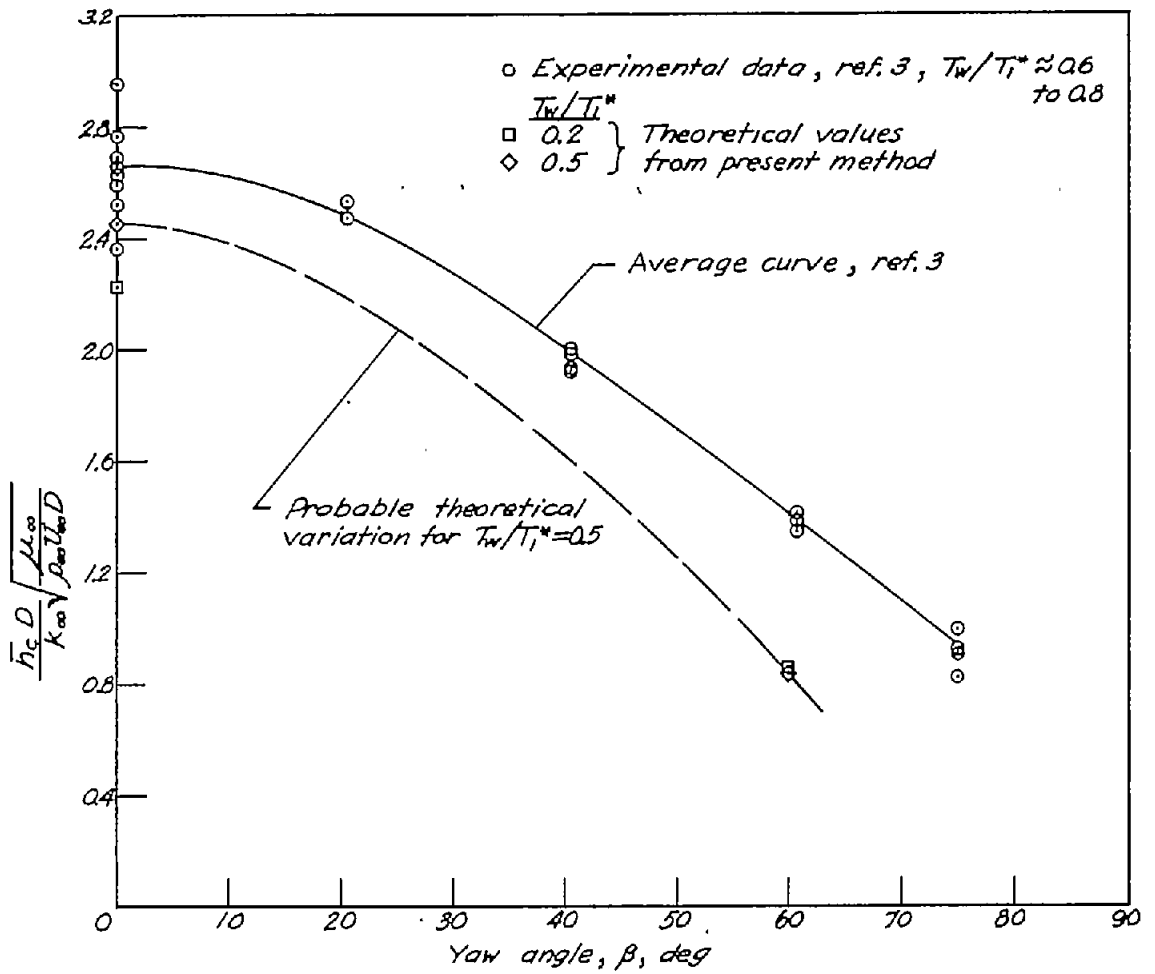

Figure 8.- The theoretical and experimental variation of the average heat-transfer parameter with yaw angle on the front half of a circular cylinder at $M_\infty \approx 6.9$ and $T_1^* \approx 1200^\circ$ R.

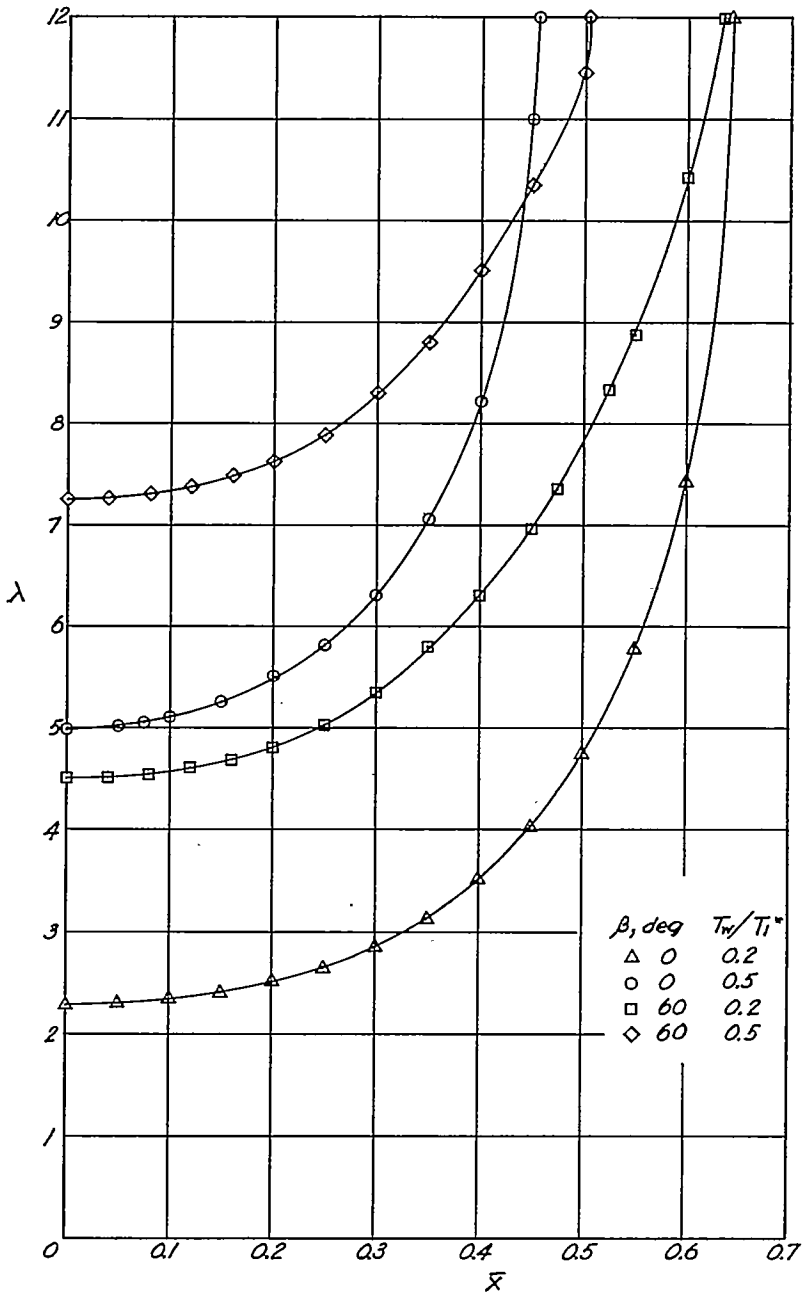

(a) Variation of λ with $\bar{x}$ for the two yaw angles and temperature ratios considered.

Figure 9.- Variation of computing parameters with arc length x/D on a circular cylinder at $M_\infty = 6.9$ and $T_1^* = 1200^\circ$ R.

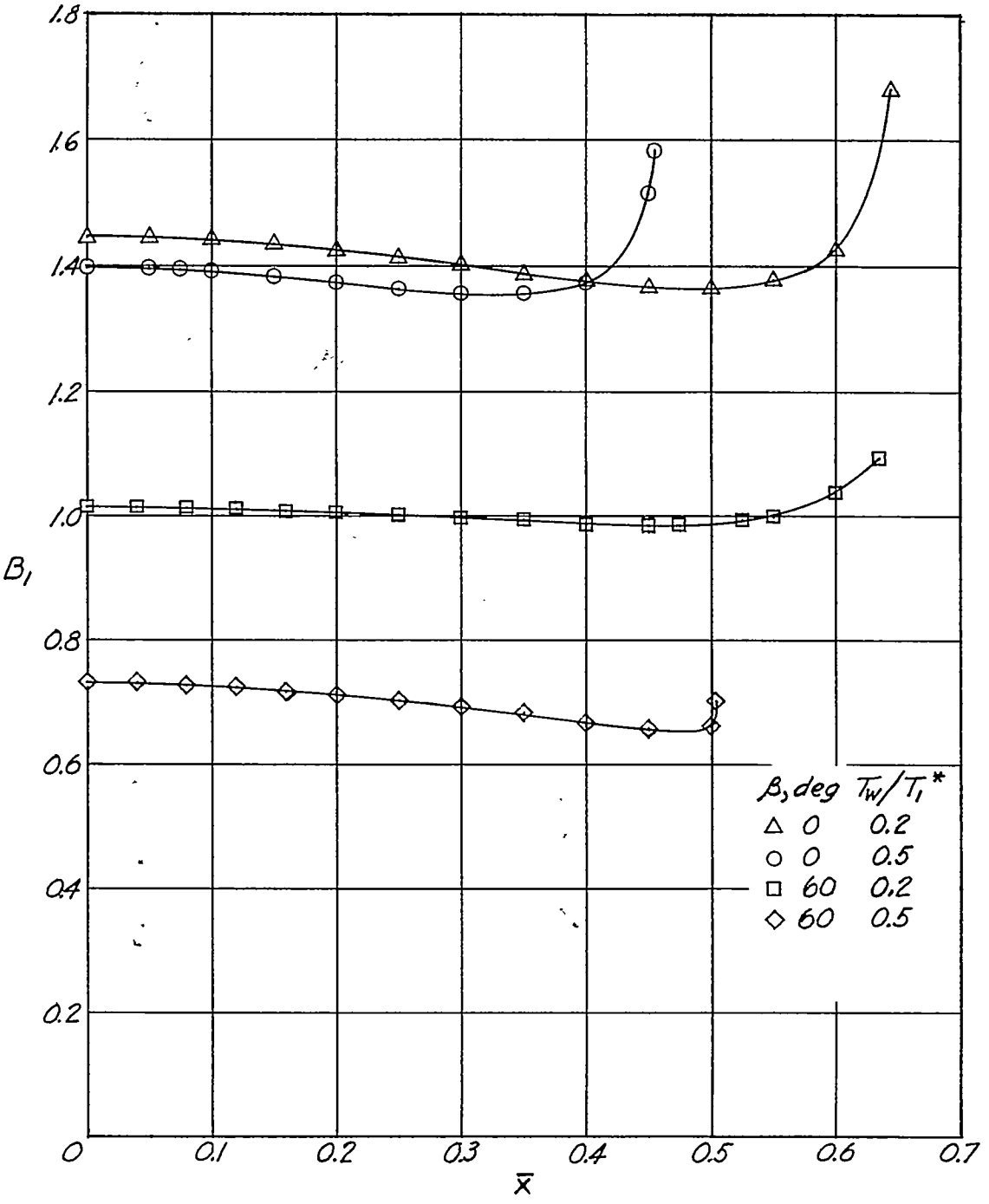

(b) Variation of B_1 with $\bar{x}$ for the two yaw angles and temperature ratios considered.

Figure 9.- Continued.

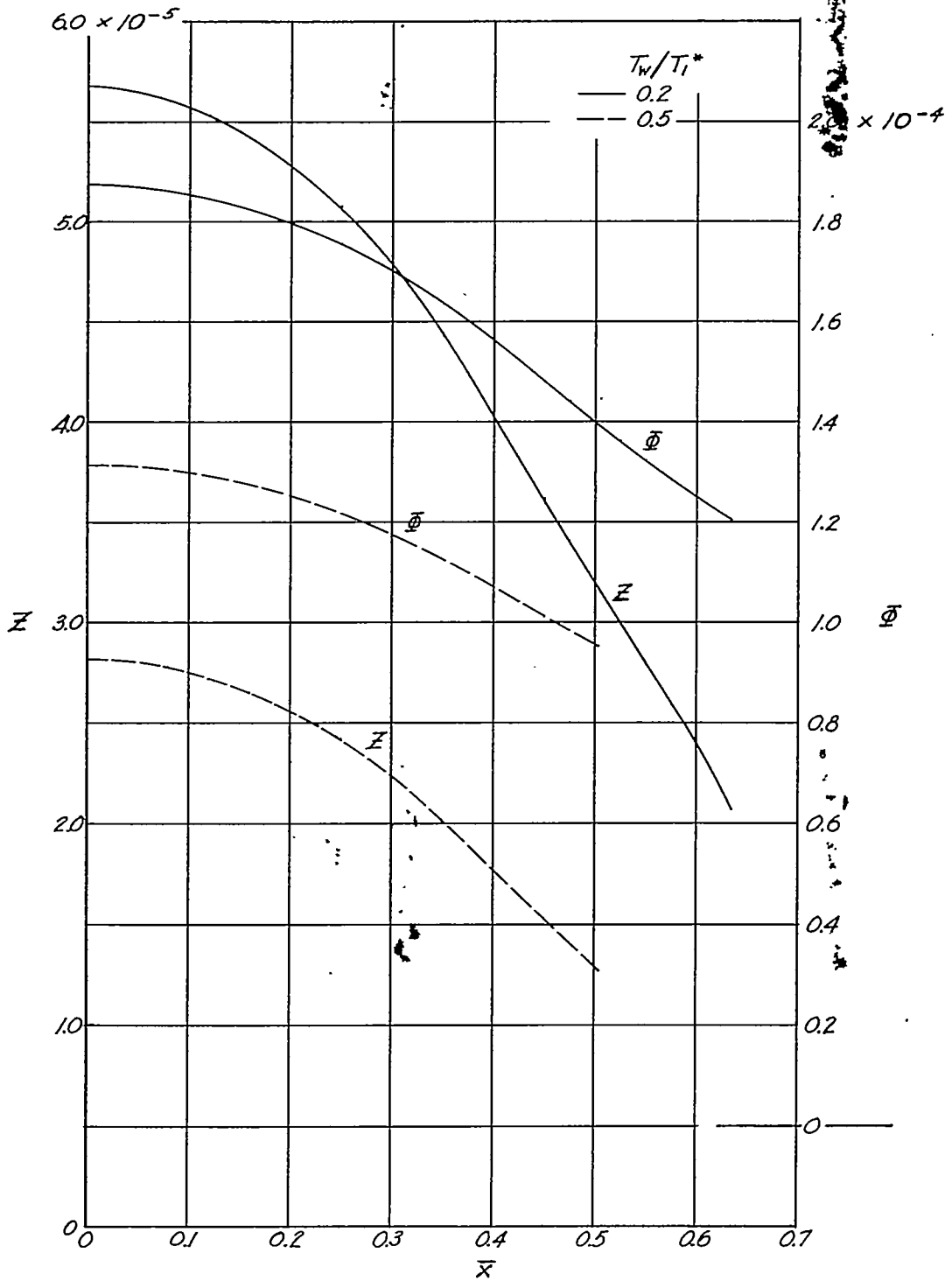

(c) Variation of Z and ϕ with $\bar{x}$ at a yaw angle of 60°.

Figure 9.- Concluded.

NACA - Langley Field, Va.